energy&fuels

Article

pubs.acs.org/EF

Fickian Diffusion in Discrete-Fractured Media from Chemical Potential Gradients and Comparison to Experiment

Joachim Moortgat*,†,‡ and Abbas Firoozabadi*,‡,¶

†School of Earth Sciences, The Ohio State University, Columbus, Ohio 43210, United States

‡Reservoir Engineering Research Institute, Palo Alto, California 94301, United States

¶School of Engineering and Applied Science, Yale, New Haven, Connecticut 06511, United States

ABSTRACT: Fickian diffusion can be an important oil recovery mechanism from fractured reservoirs by gas injection, especially when gravitational drainage is inefficient. Without diffusion, injected gas will flow predominantly through the fractures, resulting in early breakthrough and low oil recovery, but compositional gradients between the fractures and the matrix can drive considerable cross-flow. Additionally, this species exchange can lead to favorable phase behavior, such as swelling and viscosity reduction of oil in the matrix. The modeling of Fickian diffusion in fractured reservoirs has been hampered by two deficiencies in existing simulators. The first is the use of the generalized classical Fick's law for multicomponent mixtures, which violates molar balance. The second is the computation of diffusive fluxes across grid edges aligned with phase boundaries. Traditionally, diffusive fluxes are derived from gradients in compositions, computed by finite differencing of compositions in neighboring grid cells. This approach fails when one grid cell contains only gas and the neighboring cell only oil, because the compositional gradients are only defined within a single phase. This problem often occurs in fractured domains when the fractures fill with injected gas while the matrix blocks remain in single-phase oil. We implement an alternative approach, in which gradients in chemical potential are the driving force for Fickian diffusion. Unlike phase compositions, chemical potentials do not require phase identification and the gradient can be computed self-consistently across phase boundaries. Away from phase boundaries the two approaches are equivalent. We demonstrate the strengths of our implementation by simulating experiments in which CO_2 is injected in a tall vertical core surrounded by fractures. After injecting CO_2 for 22 days, 65% of the oil in place is recovered. However, modeling with a commercial simulator results in only 12% recovery, despite adjusting parameters. We present additional examples at larger scales that further confirm the promising prospects of CO_2 injection for enhanced oil recovery in fractured reservoirs and show the equivalence of the composition- and chemical-potential-based formulations in the absence of sharp phase boundaries.

■ INTRODUCTION

The growing awareness and concern regarding the ecological and economic threats posed by global warming have triggered a high interest in the sequestration of CO_2, produced by burning of fossil fuels, in either saline aquifers or oil reservoirs. The financial burden of such plans may be greatly alleviated by the growing proof that CO_2 injection may significantly improve oil recovery as a secondary or tertiary recovery mechanism in fractured reservoirs. Irrespective of the global warming aspects, recovery in many of the world's largest oil reservoirs is declining, following primary and secondary recovery. CO_2 injection is attracting the most new market interest as an enhanced oil recovery (EOR) mechanism and is, for instance, being piloted by the Department of Energy in a number of reservoirs, using geological as well as industrial sources of CO_2. In light of this, a proper understanding of CO_2 injection in oil reservoirs and saline aquifers is essential to both government and the industry. For the industry, reliable estimates of the incremental oil recovery have to justify the cost of the CO_2 supply (capture and/or transport).

Due to the exceedingly large scale of field problems, most commercial simulators employ highly simplified models that may or may not capture the essential physics. In particular, there are concerns regarding the accuracy and flexibility of finite difference methods and of dual-porosity models in modeling fracture−matrix interactions. Fickian diffusion poses further challenges that have not been resolved in dual-porosity models.[1] Even in unfractured domains, there are fundamental weaknesses in the way Fickian diffusion has been modeled in the past. The classical Fick's law has been generalized to multicomponent mixtures by considering a diagonal matrix of diffusion coefficients. However, one can easily demonstrate that a diagonal matrix of diffusion coefficients can only satisfy mass balance when all the diagonal components are identical,[2] that is when a scalar diffusion coefficient is used. By using different diagonal diffusion coefficients, diffusion will cause an unphysical molar imbalance which in turn results in pressure oscillations. Such pressure oscillations are not necessarily observed because they drive convective fluxes that will quickly equilibrate the system but, nevertheless, reduce the overall reliability of simulations using this approach. As a first step to improve the modeling of Fickian diffusion, we have implemented a model for the full matrix of composition dependent diffusion coefficients, based on irreversible thermodynamics.[3,4] By incorporating the off-diagonal diffusion coefficients, we not only satisfy molar balance but can also model various diffusion phenomena that cannot be described by classical Fick's law.[2] Dragging or coupling effects from other components can cause

Received: June 18, 2013
Revised: August 30, 2013
Published: September 4, 2013

diffusion of a species even without a gradient in its own composition (osmotic diffusion), components may not diffuse even when there is a gradient in its composition (diffusion barrier), or components can diffuse from low to high concentrations (reverse diffusion). All these effects have been demonstrated experimentally.[5]

In this work, we address another fundamental complication in modeling diffusion in multiphase flow, particularly in fractured media. Both Fick's law and our earlier improved diffusion model in terms of a full matrix of diffusion coefficients assume that the driving forces for diffusion in multiphase flow are gradients in *phase* compositions (which we refer to as the *conventional* approach). This poses a numerical problem in multiphase flow exhibiting sharp phase boundaries. This frequently occurs in heterogeneous and fractured domains. Consider gas injection into a fractured domain saturated with oil. When the fractures fill with (single-phase) gas, while the neighboring matrix blocks are saturated with (single-phase) oil, the conventional model cannot self-consistently compute the diffusive flux between the fractures and the matrix, because gradients in phase compositions cannot be defined between two different phases. In this work, we adopt an alternative formulation in which gradients in *chemical potentials* provide the driving force. This formulation in terms of chemical potential gradients and a full matrix of phenomenological coefficients has been derived in a number of earlier papers[2,6,7] but, to the best of our knowledge, has not been implemented and tested for multiphase flow in fractured porous media. The governing equations for both formulations are mathematically equivalent, but the aforementioned numerical issues at phase boundaries are resolved because chemical potentials are defined irrespective of the (number of) phases. In other words, the model predicts nearly identical results away from sharp phase boundaries but can also self-consistently describe the diffusive flux across the phase boundaries that often occur at the interfaces between fractures and matrix blocks and at discontinuities in rock permeability (e.g., layered domains).

This paper is organized as follows: first, we present our formulation for Fickian diffusion in which gradients in chemical potentials are the driving force, and clearly highlight the equivalence and the differences with respect to the conventional formulation in terms of gradients in compositions. We briefly recapitulate our discrete fracture model, summarize the main governing equations and boundary conditions, and outline our numerical implementation using higher-order finite element methods. In the second part, we present three numerical examples to illustrate powerful features of our implementation. In the first two examples, we show the equivalence of either compositional or chemical potential gradients as a driving force for Fickian diffusion in the absence of sharp phase boundaries. The first illustrates the stabilizing effect of Fickian diffusion on gravitational (and viscous) fingering instabilities, and the second considers a larger-scale extensively fractured heavy oil reservoir and demonstrates how Fickian diffusion significantly improves the oil recovery from CO_2 injection. In the third example, we verify the model by considering a rich data set provided by experiments, in which CO_2 is injected from the top of a tall cylindrical chalk core saturated with live oil and surrounded by fractures.[8−10] We construct an equation of state (EOS) model based on the Peng−Robinson EOS[11] (PR-EOS), and we compare our EOS predictions to the *pVT* experiments and the phase behavior of mixtures of CO_2 and reservoir oil. In particular, we study the aspects that affect CO_2 as an EOR candidate: the change in liquid density, viscosity, and volume as a function of the amount of CO_2 dissolved in the oil. Next, we describe the core flooding experiment and present our numerical modeling. We analyze the agreements and differences between the experimental and numerical outcomes, compare our numerical results to those obtained by a commercial simulator, and discuss some of the limitations of the latter. We end with a summary of our main conclusions.

MATHEMATICAL FORMULATION

For the sake of completeness, we recapitulate the expressions for the Fickian diffusive fluxes in terms of chemical potential gradients, and we compare to the conventional formulation in terms of gradients in (phase) compositions. Furthermore, we emphasize specific complications in implementing this model for Fickian diffusion in multiphase compositional flow in fractured porous media in the context of reservoir simulations.

Chemical Potential Gradients as Driving Force for Fickian Diffusion. On the basis of the thermodynamics of irreversible processes, the entropy strength σ of a system at constant temperature increases due to diffusive fluxes $\mathbf{J}$ as[7]

$$\sigma = -\frac{1}{T}\sum_{i=1}^{n_c} J_i \nabla \mu_i \geq 0 \tag{1}$$

in terms of the chemical potential μ_i of each species i, with n_c the total number of components. In this section, we will use bold notations for vectors $\mathbf{J} = [J_i]$, with vector components J_i indicated in italic. Similarly, matrices $\mathrm{L} = [L_{ij}]$ are in roman, with matrix components L_{ij} in italic. Equation 1 guarantees that there is no entropy production at thermodynamic equilibrium, where all chemical potential gradients vanish.

The diffusive fluxes are not independent:

$$\sum_{i=1}^{n_c} J_i = 0 \quad \text{or} \quad J_{n_c} = -\sum_{i=1}^{n_c-1} J_i \tag{2}$$

The chemical potentials are also not independent and satisfy the Gibbs−Duhem equation at (locally) constant temperature and pressure:

$$\sum_{i=1}^{n_c} x_i \nabla \mu_i = 0 \quad \text{or} \quad \nabla \mu_{n_c} = -\sum_{i=1}^{n_c-1} \frac{x_i}{x_{n_c}} \nabla \mu_i \tag{3}$$

where x_i is the mole fraction of species i. Using eqs 2 and 3, we rewrite eq 1 as follows:

$$\sigma = -\frac{1}{T}\sum_{i=1}^{n_c-1} J_i \sum_{k=1}^{n_c-1}\left(\delta_{ik} + \frac{x_k}{x_{n_c}}\right)\nabla \mu_k \tag{4}$$

For notational convenience, we define the transformation matrix

$$A_{ik} = \left(\delta_{ik} + \frac{x_k}{x_{n_c}}\right) \tag{5}$$

and the vector of independent driving forces:

$$Y_i = -\frac{1}{T}\sum_{k=1}^{n_c-1} A_{ik} \nabla \mu_k \tag{6}$$

The simplest constitutive relation between the independent fluxes J_i $(i = 1, ..., n_c - 1)$ and driving forces Y_i $(i = 1, ..., n_c-1)$ is

dx.doi.org/10.1021/ef401141q | Energy Fuels 2013, 27, 5793−5805

$$\mathbf{J} = \mathrm{L}\boldsymbol{Y} \tag{7}$$

where the matrix L contains the transport coefficients L_{ij} (i, j = 1, ..., n_c−1), called the phenomenological or Onsager coefficients.

We want to relate the Onsager to the Fickan diffusion coefficients D_{ik}^{Fick}, which appear in the relation for diffusion in which compositional gradients are the driving force (and c is the molar density):

$$J_i = -c \sum_{k=1}^{n_c-1} D_{ik}^{\mathrm{Fick}} \nabla x_k, \quad i = 1, \ldots, n_c - 1 \tag{8}$$

We therefore write

$$\nabla \mu_i = \sum_{k=1}^{n_c-1} \frac{\partial \mu_i}{\partial x_k} \nabla x_k, \quad i = 1, \ldots, n_c - 1 \tag{9}$$

The composition dependence of the chemical potentials relates to the nonideality of the fluid and can be captured in a matrix with elements Γ_{ik}:

$$\frac{\partial \mu_i}{\partial x_k} = RT \frac{\partial \ln f_i}{\partial x_k} = \frac{RT}{x_k} \Gamma_{ik}, \quad \text{with}$$
$$\Gamma_{ik} = \frac{\partial \ln f_i}{\partial \ln x_k}, \; i, \; k = 1, \ldots, n_c - 1 \tag{10}$$

We define the $(n_c - 1) \times (n_c - 1)$ diagonal matrix X with $X_{ii} = x_i$ and write eq 9 in matrix form as

$$\nabla \mu = RT \mathrm{X}^{-1} \Gamma \nabla \mathrm{x} \tag{11}$$

Combining eqs 5, 6, 7, and 11, we write the diffusion flux in terms of the Onsager coefficients and compositional gradients as

$$\mathbf{J} = -R \; \mathrm{LA} \, \mathrm{X}^{-1} \Gamma \nabla \mathbf{x} \tag{12}$$

The relation between the Fickian diffusion coefficients and the Onsager coefficients is therefore given by

$$c\mathrm{D}^{\mathrm{Fick}} = R \; \mathrm{LA} \, \mathrm{X}^{-1} \Gamma \tag{13}$$

The Fickian diffusion coefficients can also be derived from the Stefan−Maxwell diffusion coefficients $\mathcal{D}_{ij}$ for each pair of components i and j.[3] For notational convenience, we define a square matrix B^{M} as

$$B_{ii}^{M} = \frac{x_i}{\mathcal{D}_{in_c}} + \sum_{\substack{k=1 \\ i \neq k}}^{n_c} \frac{x_k}{\mathcal{D}_{ik}}, \quad i = 1, \ldots, n_c - 1 \tag{14}$$

$$B_{ij}^{M} = -x_i \left(\frac{1}{\mathcal{D}_{ij}} - \frac{1}{\mathcal{D}_{in_c}} \right), \quad i, \; j = 1, \ldots, n_c - 1; \; i \neq j \tag{15}$$

and its inverse as $\mathcal{B}^{M} = (\mathrm{B}^{\mathrm{M}})^{-1}$. In terms of $\mathcal{B}^{\mathrm{M}}$, the Fickian coefficients are given by

$$\mathrm{D}^{\mathrm{Fick}} = \mathcal{B}^{\mathrm{M}} \Gamma \tag{16}$$

such that

$$\mathrm{L} = \frac{c}{R} \mathcal{B}^{\mathrm{M}} \mathrm{X} \mathrm{A}^{-1} \tag{17}$$

Note that while the matrices $\mathcal{B}^{\mathrm{M}}$, A^{-1}, and $\mathrm{D}^{\mathrm{Fick}}$ are not symmetric, XA^{-1}, and, more importantly, L are symmetric, with positive diagonal coefficients. The symmetry of L is referred to as the Onsager reciprocal relation and is a powerful feature of this formulation.

A more convenient expression for the diffusive fluxes results from noticing that the matrices A in eq 6 and A^{-1} in eq 17 cancel, such that

$$J_i = -\frac{c}{RT} \sum_{k=1}^{n_c-1} \mathcal{B}_{ik}^{\mathrm{M}} x_k \nabla \mu_k, \quad i = 1, \ldots, n_c - 1 \tag{18}$$

The above relations were derived for a single phase in open space. For multiphase flow in porous media, the diffusive fluxes in each phase α are given in the two formulations by

$$J_{\alpha,i} = -\phi S_\alpha c_\alpha \sum_{k=1}^{n_c-1} D_{\alpha,ik}^{\mathrm{Fick}} \nabla x_{\alpha,k},$$
$$\text{versus } J_{\alpha,i} = -\frac{\phi S_\alpha c_\alpha}{RT} \sum_{j=1}^{n_c-1} \mathcal{B}_{\alpha,ij}^{\mathrm{M}} x_{\alpha,j} \nabla \mu_{\alpha,j} \tag{19}$$

where, for each phase α, S_α is the saturation, c_α the molar density, $x_{\alpha,i}$ the molar composition, $\mathrm{D}_\alpha^{\mathrm{Fick}}$ the Fickian diffusion coefficients, and ϕ the porosity (the expressions may also be divided by the tortuosity).

Both expressions in eq 19 are mathematically equivalent, but the latter is a considerable improvement in terms of numerical implementation for multiphase problems. When one grid cell is single-phase gas with composition $x_{g,i}$, and the neighboring cell is single-phase oil with composition $x_{o,i}$, for instance, the gradients $\nabla x_{g,i}$ and $\nabla x_{o,i}$ cannot be computed from differencing the compositions. The chemical potentials, however, are the same for each phase in a multiphase mixture (i.e., $\mu_{g,i} = \mu_{o,i} = \mu_i$) and can be readily evaluated as the driving force for Fickian diffusion, whether grid cells are in single-phase or in multiphase.

We note that the numerically computed fluxes from the two expressions above will be somewhat different, because the nonideality of the fluids is represented differently in the two approaches. In the conventional method, the nonideality is incorporated in the diffusion coefficients $\mathrm{D}^{\mathrm{Fick}}$, through Γ from eq 10, which are averaged between two neighboring grid cells, while in our new approach the nonideality is included in the chemical potentials themselves, that is inside the gradient operator. In terms of implementation, the chemical potentials are evaluated in both methods as part of the phase-split computations and are used either explicitly as the driving force $\nabla \mu_i$ or in describing the nonideality in Γ, so no additional computations are required in this formulation. Finally, we repeat that it is critical to consider the full matrix of compositional dependent diffusion coefficients to guarantee molar balance in either formulation.[2]

Further details of the discretized computation of the diffusive flux across edges (Figure 1) between neighboring grid cells are provided in the Appendix.

Convective Fluxes and Discrete Fracture Model. The convective fluxes for each phase α are given by Darcy's law as

$$\mathbf{u}_\alpha = \lambda_\alpha \mathrm{K}(\nabla p_\alpha - \rho_\alpha g) \tag{20}$$

in terms of phase pressure p_α, mass density ρ_α, gravity g, and mobility $\lambda_\alpha = k_{r,\alpha}/\nu_\alpha$, with relative permeability $k_{r,\alpha}$ and viscosity ν_α (note that we use ν_α, rather than μ_α for the viscosity, to avoid confusion with the chemical potentials μ_i). K is the absolute

dx.doi.org/10.1021/ef401141q | Energy Fuels 2013, 27, 5793−5805

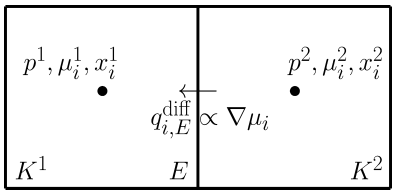

Figure 1. Illustration for the computation of the chemical potential gradient across edge E between grid cells K^1 and K^2.

permeability. Note that, from here on, vector notation refers to *spatial* components $\mathbf{u}_\alpha = (u_{\alpha,x}, u_{\alpha,y}, u_{\alpha,z})$, and similarly for $\mathbf{J}_{i,\alpha}$.

In earlier work,[12] we have presented a discrete fracture model that allows for any configuration of fractures and overcomes the limitations of single- and dual-porosity fracture models.[13,14] Without repeating the details of the formulations, we outline here the key elements of our model. The basic assumption is that fractures have a high transverse permeability that instantaneously equilibrates the fluid in the fracture with that in the immediate neighborhood in the matrix. With this assumption, the explicit computation of the fracture−matrix flux is avoided. We combine a fracture grid cell with two small slices of the matrix blocks on either side into a large computation element. We refer to this as the cross-flow equilibrium approach and to these fracture-containing computational elements as cross-flow (CF) elements. The CF elements have one average pressure and a composition and density that are a mixture of the fracture and matrix fluids.[15] In the direction perpendicular to the fracture, the flux across the edge of a CF element is computed the same way as between two matrix grid cells. In the direction parallel to the fracture, the flux across a CF element edge is the properly integrated sum of the fracture and matrix contributions.

The cross-flow equilibrium approach combines the benefits of the single- and dual-porosity models, while avoiding their deficiencies. Similar to a single-porosity simulation, we can have any configuration of discrete fractures and treat physical interactions between the fracture and matrix explicitly. In the dual-porosity approach, fractures are assumed to have a sugar-cube configuration and interactions between fractures and the matrix have to be described by semiempirical transfer-functions. Single-porosity models are generally computationally inefficient, because the small fracture grid cells require exceedingly small time-steps, and the high contrast in fracture and matrix properties (particularly the permeability) makes the system of equations ill-conditioned. These efficiency issues are alleviated in our approach by using large computational elements with appropriately averaged properties. While fractures may have an aperture of the order of millimeters or less, the CF elements can have a width of 10−20 cm and reproduce identical results.[12,15] This approximation is valid for conventional reservoirs with matrix permeabilities $\gtrsim$1 md, but it breaks down for very tight formations, such as shale. We note that although we consider a single composition for the CF elements, we still allow for different relative permeabilities and capillary pressures for the fracture and matrix contributions.

Mass Transport and Pressure Equation. With the diffusive and convective fluxes defined in the previous sections, we can write the continuity equation in terms of the total molar density c and overall molar composition of the multiphase mixture, z_i, as

$$\phi \frac{\partial c z_i}{\partial t} + \nabla\cdot \mathbf{U}_i = F_i, \quad i = 1, \ldots, n_c \tag{21}$$

$$\mathbf{U}_i = \sum_\alpha (c_\alpha x_{i,\alpha} \mathbf{u}_\alpha + \mathbf{J}_{i,\alpha}), \quad i = 1, \ldots, n_c \tag{22}$$

where F_i is a sink/source term that may represent injection or production wells.

We adopt an explicit evolution equation for the pressure:[16,17]

$$\phi\kappa_T \frac{\partial p_o}{\partial t} + \sum_{i=1}^{n_c} \overline{v}_i(\nabla\cdot \mathbf{U}_i - F_i) = 0 \tag{23}$$

where κ_T and $\overline{v}_i$ are the total compressibility and total partial molar volumes of the multiphase mixture, respectively. When formation compressibility is significant, κ_T and ϕ depend weakly on pressure (neglected in this work). The oil phase pressure is chosen as a reference when capillarity is considered.

The system of equations is supplemented by thermodynamic equilibrium relations that guarantee the equality of chemical potentials of each component i in all phases α. As boundary conditions, we assume impermeable walls except in production wells, where we can have either a constant pressure or constant production rate. Injection wells are treated as source terms F_i.

■ NUMERICAL IMPLEMENTATION

We solve the multiphase flow equations with a choice of higher-order finite element methods that are particularly well suited for fractured reservoirs. Specifically, we employ the mixed hybrid finite element (MHFE) method to simultaneously and to the same order of accuracy solve for globally continuous pressure and flux fields, and a higher-order discontinuous Galerkin (DG) discretization of the continuity equation. In the DG method, any order of approximation can be used in each grid cell and the variables (compositions) can be discontinuous across edges, which is advantageous in fractured and heterogeneous domains, as well as across phase boundaries. By using a higher-order (bilinear) discretization for the mass transport update, we achieve a higher order convergence, which translates into low numerical dispersion or, equivalently, accurate solutions on coarse grids and at large time-steps.[18] The two methods are coupled in an implicit pressure explicit composition (IMPEC) scheme, which takes advantage of the weak coupling between the pressure equation and mass transport and allows larger time-steps for the global pressure solution than for the more rapidly varying compositions.

Our full algorithm for compositional multiphase flow simulations is constructed as follows:

1. From a user-provided overall composition throughout the reservoir, temperature, and initial pressure at the bottom of the domain, hydrostatic equilibrium is established.

2. On the basis of the overall composition, temperature, and pressure, a thermodynamic phase stability analysis is carried out.

3. When the phase is unstable, EOS-based phase-split computations are performed to determine the phase amounts, phase compositions $x_{\alpha,i}$, and chemical potentials μ_i. These phase-split computations use the PR-EOS with volume translation[11] for pure hydrocarbon phases, or our cubic-plus-association EOS when polar molecules such as water or asphaltenes are present.[18,19]

4. From the phase compositions, the mobilities (relative permeability and viscosity), densities, saturations, capillary pressures, and phenomelogical coefficients are derived.

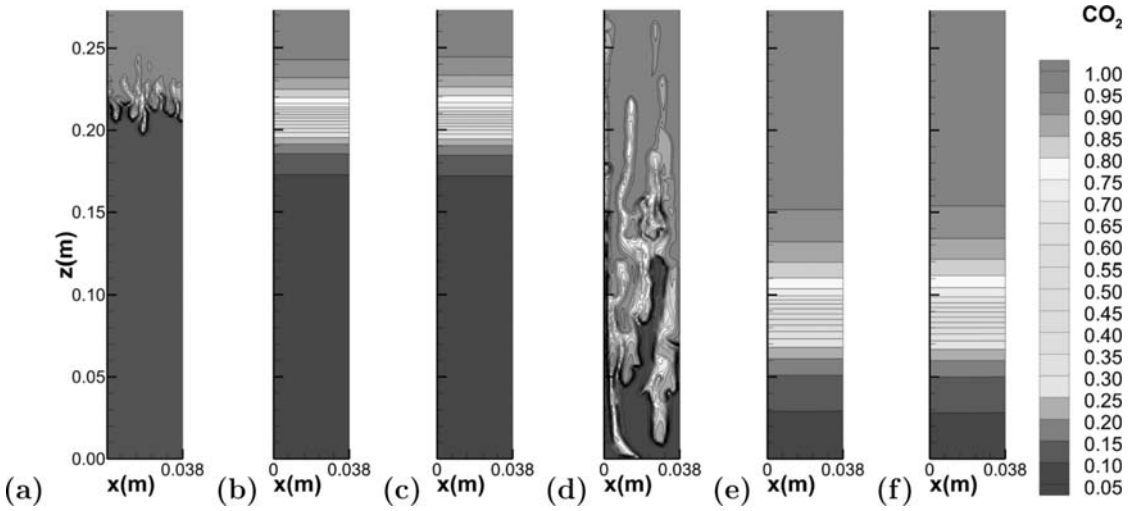

Figure 2. Example 1: Overall CO_2 composition (molar fraction) at 20% (a–c) and 60% (d–e) PVI. Simulations without diffusion (a, d), with Fickian diffusion based on compositional gradients (b, e), and with Fickian diffusion based on chemical potential gradients (c, f).

5. The capillary pressure gradients are updated and the diffusive fluxes are computed from eq 19 by differencing the chemical potentials between neighboring elements and projecting the coefficients onto the element edges (eq 30).

6. A linear system of equations is constructed for the backward-Euler time update of the pressures and fluxes using the MHFE method, and solved by an off-the-shelf direct linear solver. We have developed a fractional flow formulation in terms of the *total* flux.[20] After solving for the total flux, the phase convective fluxes are constructed as a postprocess, using the upwind effective mobilities with respect to the phase fluxes.

7. With the new convective and diffusive fluxes, the explicit DG mass transport update (forward-Euler) is performed to find the new overall compositions.

8. A slope limiter is used to avoid the spurious oscillations that may occur in higher-order methods.

9. An adaptive time-stepping routine determines the CFL condition for the next iteration.

10. The loop returns to step 2.

■ NUMERICAL EXAMPLES

We present three numerical examples to verify our new implemention for Fickian diffusion. The first two examples demonstrate that when single-phase regions are separated by a two-phase transition zone, the formulation in terms of chemical potential gradients is equivalent to the conventional approach in terms of compositional gradients. The last example considers a problem where the conventional modeling of diffusion breaks down in computing the diffusion flux across a sharp discontinuity between two single-phase regions. Specifically, we model an experiment in which CO_2 is injected in a fractured core, such that the fractures quickly fill with single-phase gas, while the (matrix) core is still in single-phase oil. This type of problem cannot be simulated reliably by diffusion models based on compositional gradients. All three examples are at (high) reservoir pressure and for CO_2 injection, where the surface tension is low and CO_2 has a high solubility in the oil. At these conditions, we can safely neglect the effect of capillary pressure.

Example 1. In this example, we verify the equivalence of the formulations for Fickian diffusion on the basis of either gradients in compositions or gradients in chemical potentials for a problem that does not involve sharp phase boundaries. We simulate injection of supercritical CO_2 in a 2D diametrical cross section of an oil-saturated core with 1.9 cm radius and 27 cm length. In an earlier work we modeled this problem in more detail.[21] The oil composition and other relevant parameters are given in that paper, but in this example we do not consider connate water and use larger diffusion coefficients (they are not reduced by tortuosity or to account for near-critical conditions).

This problem is interesting because at the temperature of 332 K and pressure of 441 bar the CO_2 density (0.92 g/cm^3) is higher than the oil density (0.74 g/cm^3), so injection from the top could be unstable to gravitational fingering. Fickian diffusion provides a restoring force for such instabilities: when a finger starts to develop, compositional gradients develop between the finger and the surrounding oil. Diffusion of components from high to low concentrations has the potential to smoothen such compositional gradients and the associated fingering instabilities (for viscous fingering as well). This process may be the most important feature of Fickian diffusion in *homogeneous* domains. Whether or not diffusion can stabilize the instability depends on the relative importance of the density difference driving the instability, the magnitude of the diffusion coefficients, and the injection rate. Another important parameter is the rock permeability, which determines the propagation speed of fingers and the associated time-scale for diffusion to stabilize the flow. In this example the permeability is relatively high at 221 md. The porosity is 13%, and we inject one pore volume from the top at 68% PV/day. To obtain converged results and clearly distinguish physical from numerical dispersion, we perform the simulations on a very fine 38 × 271 element grid. Injection is uniformly from the top, and production is from the bottom-center at a constant pressure.

Figure 2 shows the overall CO_2 composition at 20% and 60% PVI for three simulations: in the first, Fickian diffusion is neglected, and the second and third are based on the conventional diffusion formulation in terms of compositional gradients, and our implementation with chemical potential gradients as the driving force, respectively. From panels a and c of Figure 2, we find that, without a restoring force, pronounced

gravitational fingers will develop due to the high density contrast between the injected supercritical CO_2 and the oil. For the magnitude of the diffusion coefficients considered here, Fickian diffusion effectively stabilizes the instability and facilitates piston-like displacement throughout the core. Because both the convective and diffusive fluxes are strongly composition dependent, the Péclet number varies significantly throughout the domain from $\sim 10^{-1}$ far from the front to $\sim 10^{-3}$ at the front, indicating that the flow is diffusion dominated. Diffusion prevents the early breakthrough of gravitational fingers, which results in an increase in oil recovery of 25%, as shown in Figure 3. By comparing the other panels in Figure 2

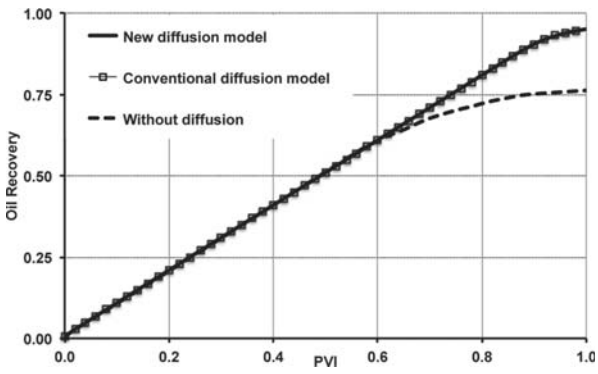

Figure 3. Example 1: Oil recovery (illustrating that the diffusive flux from compositional gradients and chemical potential gradients gives nearly identical results in this example).

and the oil recoveries, we also find that, in the absence of sharp phase discontinuities, both formulations for Fickian diffusion yield identical results.

Example 2. Next, we consider the importance of Fickian diffusion in a larger-scale extensively fractured heavy oil reservoir. Specifically, the domain size is 10 m × 10 m with 40 cm × 40 cm matrix blocks, surrounded by 1 mm fractures. The matrix blocks have a porosity of 8% and a permeability of 1 md, while the fracture permeability is 400 d, such that the effective permeability of the entire domain is ∼1 d. In both this and the next example, the effective permeability is dominated by the fractures, while most of the porosity is in the matrix, which is equivalent to a Nelson II classification of naturally fractured reservoirs.

The domain is initially saturated with a heavy viscous oil with composition and other parameters given in Table 1. The nonzero binary interaction coefficients (BIC's) are 0.1 for CO_2, N_2, and H_2S with respect to all other components, while the BIC's for methane with respect to component j are computed from $K_j = 0.0289 + 0.0001633 \times MW_j$, and tuned to 0.145 for the residue. The viscosities are computed from the LBC correlation.[22] The temperature is 381 K, and the pressure at the bottom of the domain is 376 bar, which is well over the saturation pressure of the oil (51 bar). At this condition, CO_2 has a high solubility in the oil (75 mol %). Fickian diffusion is important in exchanging CO_2 and oil-components between fracture and matrix, and the dissolution of CO_2 leads to favorable phase behavior. The initial oil has a viscosity of 122 cP, but mixing with CO_2 reduces the viscosity to as little as 4.5 cP at maximum dissolution (Figure 4a). At the same time, dissolution of CO_2 swells the oil volume by up to 50% (Figure 4b), which expels oil from the matrix and into the fractures. We also note that potential reinfiltration of oil from the fractures back into the matrix blocks is accounted for automatically in our discrete fracture model.

The oil has a density of 0.976 g/cm^3, and the CO_2 density and viscosity are 0.653 g/cm^3 and 0.035 cP, respectively (at T = 381 K and p = 376 bar). We assume quadratic relative permeabilities with equal end-points of 0.4 and a residual oil saturation of 50%. Because CO_2 has a high solubility in the oil and the oil does not readily evaporate, the fractures remain in two-phase and diffusion can be modeled with a conventional method based on phase compositions, as well as with the formulation in terms of gradients in chemical potential.

We carry out simulations on a 99 × 99 grid, such that each matrix block is discretized by 9 elements. The cross-flow elements that contain the fractures have a width of 2 cm, and we inject 50% PV of CO_2 at a rate of 25% PV/yr from the top-right fracture and produce from the bottom-left fracture, as indicated by circles in the figures. Figure 5 shows the overall CO_2 composition at 15% PVI for a simulation without Fickian diffusion, a simulation with diffusion based on the conventional approach, and a simulation with diffusion from our new implementation. Figure 6 shows the corresponding oil viscosity. The first general observation is that both approaches to model Fickian diffusion produce comparable results because there are no sharp phase boundaries. More importantly, we find that Fickian diffusion significantly improves the sweep of the fractured domain. The main purpose of diffusion is to drive the injected gas from the fractures into the matrix. Once CO_2 dissolves in the matrix oil, it can reduce the oil viscosity (Figure 6), which increases the convective flow of oil, and swell the oil volume, expelling it from the matrix. In other words, the diffusive fluxes do not need to traverse the full matrix block to have a beneficial impact. When diffusion is neglected in numerical simulations, there is no efficient transfer of CO_2 into the matrix blocks and oil recovery is only from slow gravitational drainage, hindered by the high oil viscosity. The

Table 1. Example 2: Fluid Characterization[a]

species	z_i^0	ω	T_c (K)	p_c (bar)	M_w (g/mol)	s
CO_2	5.96	0.239	304	74	44	−0.177
N_2	1.81	0.039	126	34	28	−0.289
H_2S	8.09	0.081	373	89	34	−0.239
C_1	7.13	0.011	191	46	16	−0.154
C_2−C_3	7.91	0.136	349	44	40	−0.090
iC_4,nC_4,iC_5,nC_5,C_6	11.12	0.245	466	34	72	−0.041
C_7−C_{11}	11.46	0.460	596	23	128	0.065
C_{12+}	46.52	1.111	1006	6	711	0.374

[a]Initial composition (mole %), z_i^0; acentric factor, ω; critical temperature, T_c; critical pressure, p_c; molar weight, M_w; volume translation, s.

dx.doi.org/10.1021/ef401141q | Energy Fuels 2013, 27, 5793−5805

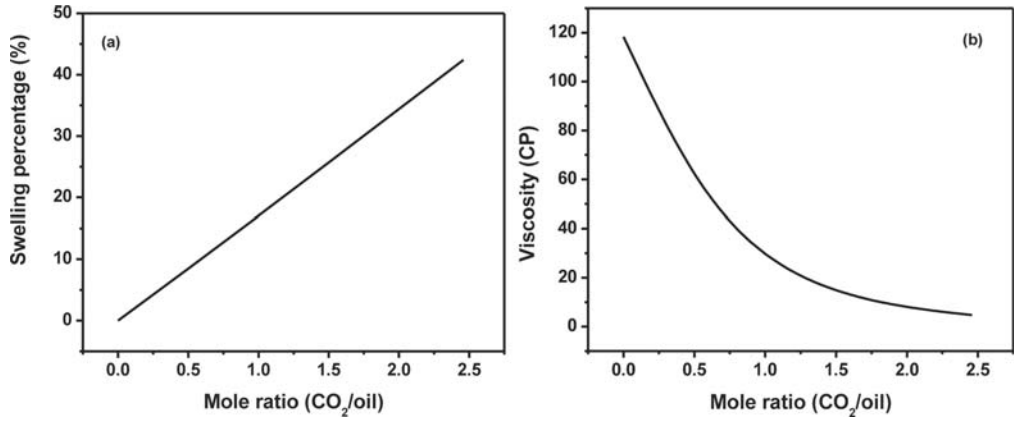

Figure 4. Example 2: Swelling (a) and viscosity reduction (b) upon mixing of initial oil with increasing fractions of CO_2.

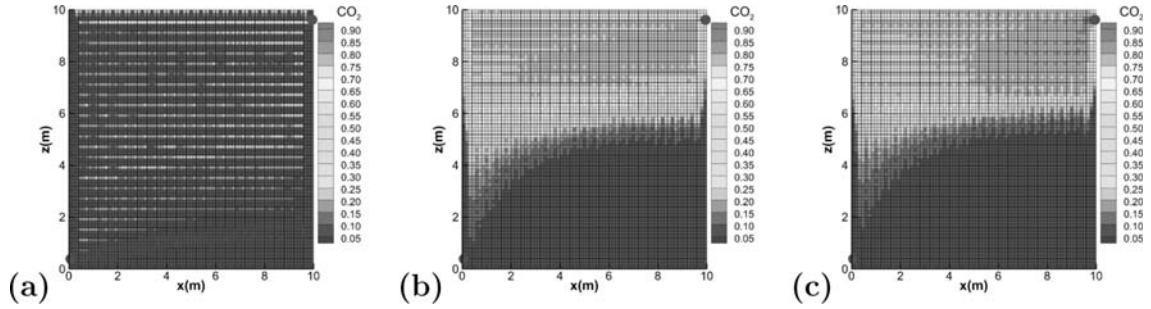

Figure 5. Example 2: Overall molar fraction of CO_2 at 15% PVI without Fickian diffusion (a), with a conventional diffusion model (b), and with a chemical potential diffusion model (c).

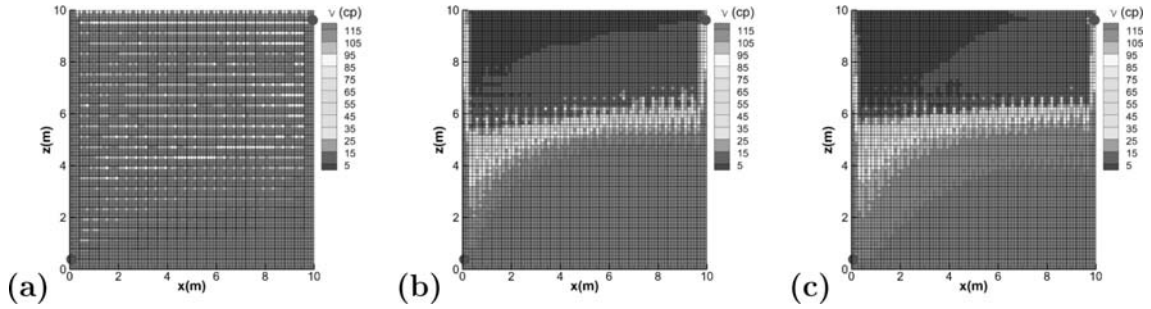

Figure 6. Example 2: Oil-phase viscosity (cp) at 15% PVI without Fickian diffusion (a), with a conventional diffusion model (b), and with a chemical potential diffusion model (c).

13% oil recovery without diffusion in Figure 7 is mainly from the fractures. When Fickian diffusion is accounted for, the oil recovery is increased to 36% because of the viscosity reduction and swelling. This example demonstrates the potential importance of Fickian diffusion in fractured heavy oil reservoirs, and the corresponding need for rigorous modeling capabilities.

Example 3. To verify the new formulation for Fickian diffusion, we model the experimental data from a Ph.D. theses by Darvish.[10] In the experimental setup, a chalk core with diameter of 46 mm and length of 600 mm is placed in the center of an empty cylinder with inside diameter of 50 mm (illustrated in Figure 8a). The core is a sample from the Faxe outcrop in Denmark and representative of the North Sea fractured chalk reservoirs. It has a permeability of 4 md and porosity of 44%. The empty annulus around the core represents a 2 mm wide fracture surrounding a matrix block.

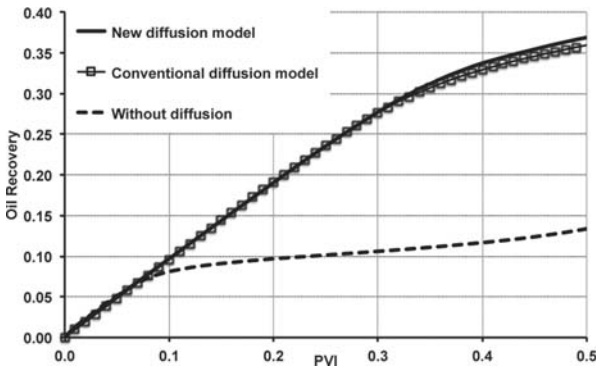

Figure 7. Example 2: Oil recovery.

Initially, the core and the cylinder are saturated with live reservoir oil. Our PR-EOS characterization of the oil is

dx.doi.org/10.1021/ef401141q | *Energy Fuels* 2013, 27, 5793−5805

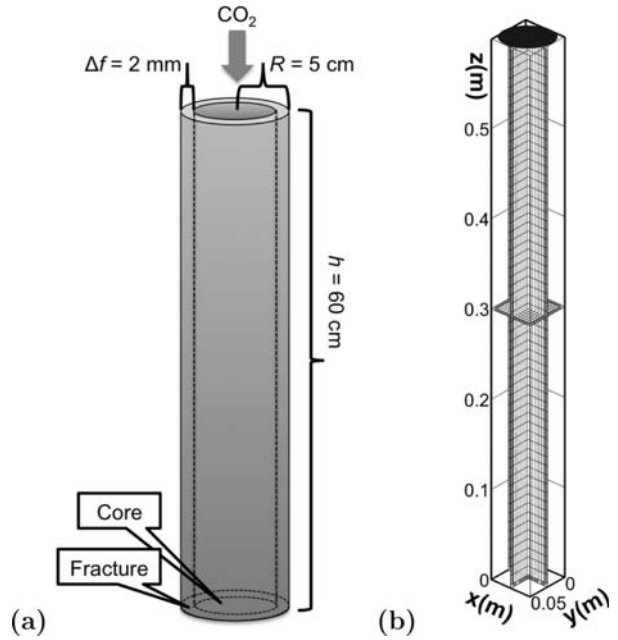

Figure 8. Example 3: Experimental setup: a cylindrical chalk core surrounded by 2 mm empty annulus representing a fracture (a). Computational grid projected on the *x*, *y*, and *z* planes (b), with uniform injection from the top fracture, and production from 21 evenly distributed elements in the bottom fracture.

provided in Table 2 and is tuned to match the experimental data.[10] The nonzero BIC's are 0.15 for CO_2 with respect to all other components. For methane, the BIC's are given by the relation in Example 2, with the residue tuned to 0.03. The latter adjustment, together with the values of the acentric factor and critical pressure of the residue, are used to match the bubble-point pressure of 242 bar. The volume shift of the residue is tuned to match the density of the original oil, and the volume shift of CO_2 to match the density of the oil mixed with CO_2. Because the initial oil has a low CO_2 concentration, the adjustment of the CO_2 volume shift does not affect the density of the pure oil. The critical volume of the residue can be tuned to match the viscosity from the LBC[22] correlation, or alternatively the corresponding states viscosity model[23] can be tuned with one adjustable parameter. Both viscosity models provide comparable results for this example. These are the only adjustable parameters in our EOS phase behavior modeling.

Table 2. Example 3: Fluid Characterization[a]

species	z_i^0	ω	T_c (K)	p_c (bar)	M_w(g/mol)	s
CO_2	0.83	0.240	304	74	44	0.100
C_1–N_2	44.27	0.011	190	46	16	−0.154
C_2	7.56	0.100	305	49	30	−0.100
C_3	4.21	0.150	370	42	44	−0.085
C_4	3.15	0.190	420	38	58	−0.072
C_5	2.19	0.240	466	34	72	−0.043
C_6	2.07	0.300	507	30	86	−0.015
C_7–C_9	8.21	0.510	546	28	108	0.038
C_{10}–C_{15}	11.58	0.670	631	20	166	0.115
C_{16}–C_{22}	5.51	0.870	717	16	247	0.169
C_{23}–C_{34}	4.65	1.060	797	14	336	0.223
C_{35}–C_{41}	3.34	1.280	907	13	484	0.268
C_{42+}	2.43	1.000	1029	7	659	−0.250

[a]Initial composition (mole %), z_i^0; acentric factor, ω; critical temperature, T_c; critical pressure, p_c; molar weight, M_w; volume translation, s. Note that generally the volume shift of the heavy components increases, but we have chosen here (and in the lumped characterization in Table 3) to tune the oil density with a single parameter. An alternative approach would be to slightly reduce the volume shifts of several of the heavier components, such that the residue still has the highest volume shift. The impact of such different characterizations on the main simulation results is minimal.

Figure 9 shows that our EOS characterization accurately reproduces the pressure dependence of the single-phase and two-phase densities and the oil volume. The measured oil density and viscosity upon mixing with CO_2 (Figure 10) do not agree as well with the EOS predictions, particularly near the saturation pressure. We suspect that this may be partly due to experimental error, because similar North Sea oils show a slight increase in single-phase oil density from CO_2 dissolution, rather than the large density decrease measured here. EOS predictions for the oil volume change due to CO_2 dissolution, shown in Figure 10c, suggest up to 15% swelling in the single-phase region, with volume shrinkage at high CO_2-to-oil ratios, due to evaporation of light components into a CO_2-rich gas phase. To speed up the simulations, we lump some of the components together and use the tuned 9 (pseudo)component characterization in Table 3. The BIC's are as for the full characterization except for the BIC of methane with respect to the residue, which is tuned to 0.08.

The experiment was carried out at reservoir pressure (300 bar) and temperature (130 °C), and CO_2 was injected into the cylinder from the top with oil produced from the bottom at a constant pressure. For the first 30 min the injection rate was kept at a high rate of 5.6 cm^3/min to produce the oil in the fracture, and then it was reduced to 0.1 cm^3/min for the next 22 days to recover the matrix oil (at which time the experiment was terminated for practical reasons, but the recovery was still increasing).

For our simulations, we consider a 3D 50 mm × 50 mm × 600 mm domain with 2 mm fractures on all the boundaries with a permeability of K_f = 25,000 md. We verified that the results do not change for $K_f \gtrsim 10$ d. However, at much higher K_f, the matrix system of equations becomes ill-conditioned due to the large fracture aperture with respect to the core size, which does not allow very wide CF elements. We use a fine 13 × 13 × 61 element grid (Figure 8b), such that the grid cells in the matrix have roughly the same size as the 4 mm wide CF elements that contain the fractures, and the simulation results are fully converged.

The simulations are initialized by saturating the cross-flow elements with CO_2 and 0.5 mol % oil, such that all components are present to compute the initial diffusion rate. This initial state represents the experiment after the high-rate flushing out of the fractures. Next, we inject 8 PV of CO_2 uniformly from the top fracture in 22 days (i.e., 0.36 PV/day). Production is at a constant pressure of 300 bar from 21 evenly distributed grid cells in the bottom fracture. Because of the strong phase behavior, we consider linear relative permeabilities in both fracture and matrix with unit end-point for oil. We consider a 0.4 end-point relative permeability for the CO_2-rich gas phase to represent the wettability alteration by CO_2.[24,21] However, we carried out additional simulations, varying the end-points from 0.2 to 1, and we find that the results are not sensitive to the relative permeability, because the main driving force is diffusion rather than convection (as discussed below). Because the oil is

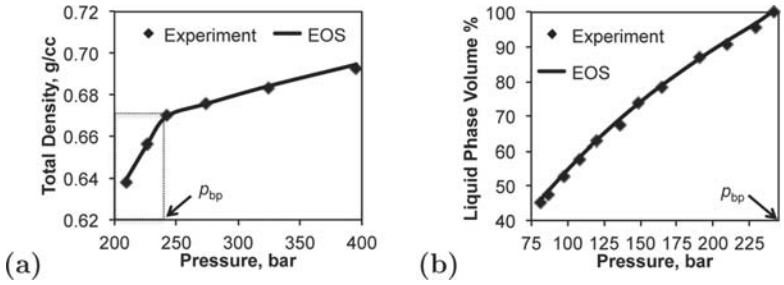

Figure 9. Example 3: Measurements and EOS computations for the total density (a) and oil volume (b) versus pressure.

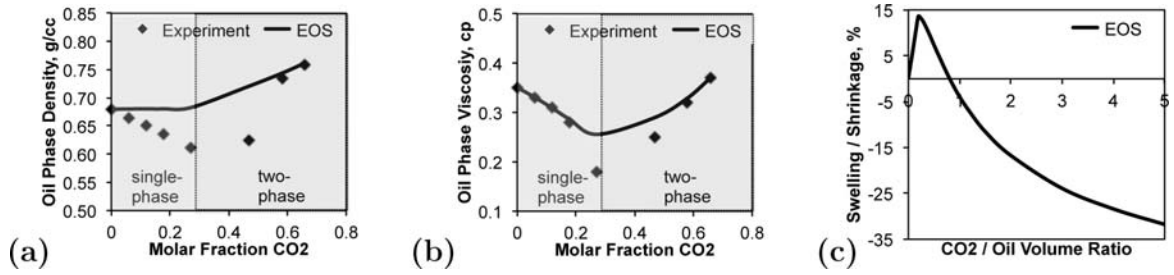

Figure 10. Example 3: Measurements and EOS computations for the oil density (a) and viscosity (b), and EOS predictions for the oil volume upon mixing with CO_2 (c).

Table 3. Example 3: Lumped Fluid Characterization[a]

species	z_i^0	ω	T_c (K)	p_c (bar)	M_w(g/mol)	s
CO_2	0.83	0.239	304	74	44	0.020
C_1-N_2	44.27	0.011	190	46	16	−0.154
C_2-C_3	11.77	0.118	328	47	35	−0.095
C_4-C_6	7.41	0.234	458	34	70	−0.047
C_7-C_9	8.21	0.370	566	26	108	0.038
$C_{10}-C_{15}$	11.58	0.595	651	19	166	0.115
$C_{16}-C_{22}$	5.51	0.870	717	16	247	0.169
$C_{23}-C_{34}$	4.65	1.060	797	14	336	0.223
C_{35+}	5.77	1.100	958	10	558	0.010

[a]Initial composition (mole %), z_i^0; acentric factor, ω; critical temperature, T_c; critical pressure, p_c; molar weight, M_w; volume translation, s.

light and will be completely evaporated when multiple (local) PV of CO_2 are passed through a grid cell, we assume zero residual oil saturation (and verified that the results do not change for residual oil saturations of up to 25%).

Figure 11 shows results for the gas saturation throughout the core after injecting one and eight pore volumes of CO_2, for simulations with and without Fickian diffusion. The overall CO_2 composition throughout the domain at the same times is shown in Figure 12. Without diffusion, there is only slow gravitational drainage from the top, while diffusion drives considerable species exchange, particularly from the vertical fractures on the sides. In Figure 12, we see that CO_2 has already reached all parts of the core by 1 PVI.

Fickian diffusion can significantly increase the oil recovery from fractured domains, because of the cross-flow between fractures and the matrix. Figure 13 shows our computed oil recoveries, as well as the measured data. The experimental results show a steep initial oil recovery, which slowly flattens off after about 2 PVI. We see the same trend in our simulations with Fickian diffusion, and we interpret the initial steep recovery as the fast production of the light oil components through diffusion. Figure 14 shows the compositions of C_1-N_2, C_2-C_3, and C_4-C_6 in the produced gas phase after flashing to surface conditions and subtracting the high CO_2 fraction, as well as the CO_2 mole fraction in the gas phase itself (note that this means that the vertical scale for C_1-N_2, C_2-C_3, and C_4-C_6 is different for the figures with and without diffusion). The early production of light components in Figure 14a was also measured in the experiments[10] and strongly supports Fickian diffusion as the dominant driving force in this experiment. The fact that our simulated oil recovery with Fickian diffusion is somewhat lower than the experimental data could be due to the uncertainty in the oil density and viscosity upon mixing with CO_2. The purpose of this example is not necessarily to perfectly reproduce these experimental data, but rather to demonstrate (1) the potential importance of diffusion in fractured media and (2) that we can model the diffusive flux across the phase boundary at the fracture−matrix interface with our formulation in terms of chemical potential gradients. Our simulations reproduce the measured early production of light components and show the same trend in the oil recovery, particularly as compared to simulations without Fickian diffusion.

When diffusion is neglected, a gravitational drainage front slowly moves through the core (Figures 11 and 12), and the composition of the produced gas is more or less constant (Figure 14b). The final oil recovery is only around 14%. We can compare the oil recovery without diffusion to the analytical prediction of the maximum drainage rate of an oil-saturated matrix block, surrounded by gas, from only gravity:[25]

$$q_{o,\text{drainage}} = \frac{K_m k_{r,o}^0}{\nu_o} g \Delta\rho \tag{24}$$

which for K_m = 4 md, $k_{r,o}^0$ = 1, ν_o = 0.34 cP, and $\Delta\rho$ = 0.14 g/cm^3 gives a rate of only 0.13 cm/day, or about 5% oil recovery in 22 days. The simulated oil recovery without diffusion is somewhat higher due to phase behavior, such as volume swelling and an increase in oil density in the top of the core, but clearly the oil recovery from only viscous and gravitational forces would be low.

dx.doi.org/10.1021/ef401141q | Energy Fuels 2013, 27, 5793−5805

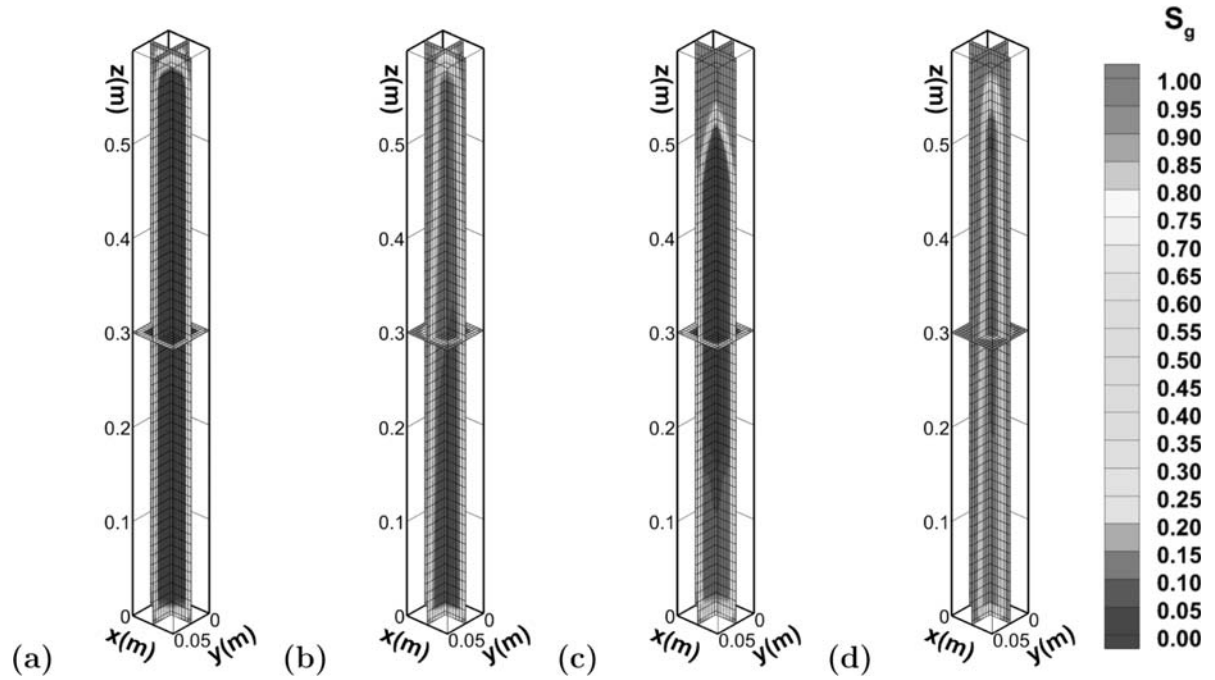

Figure 11. Example 3: Gas saturation at 1 PVI (a, b) and 8 PVI (c, d). Simulations without diffusion (a, c), and with Fickian diffusion (b, d).

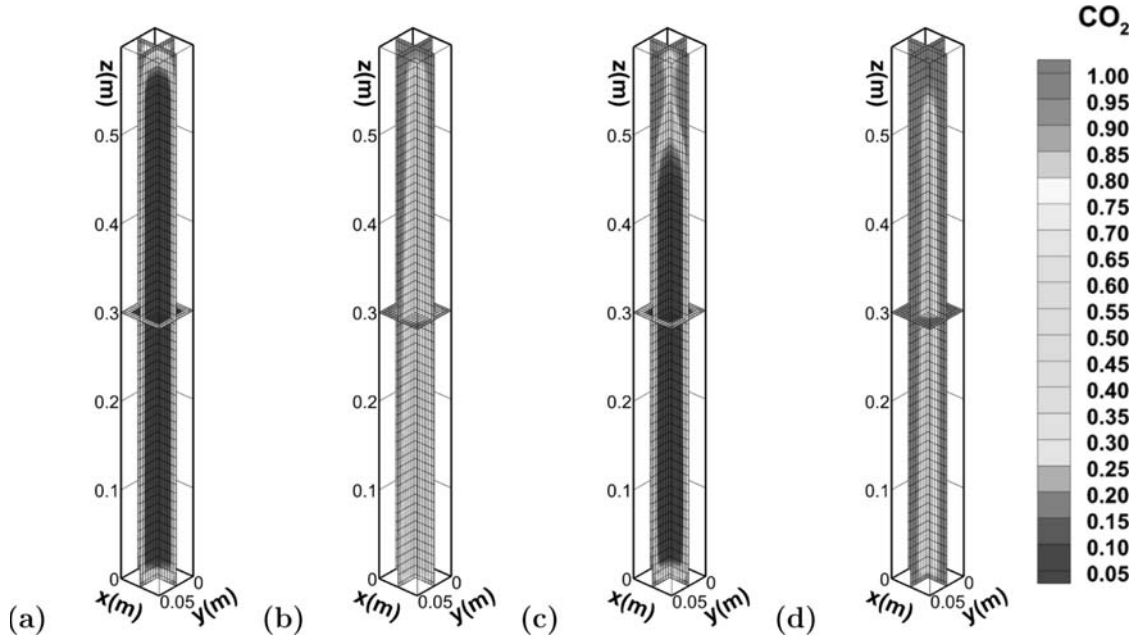

Figure 12. Example 3: Overall CO_2 composition at 1 PVI (a, b) and 8 PVI (c, d). Simulations without diffusion (a, c), and with Fickian diffusion (b, d).

Comparison to Other Simulators. This experiment is a prime example of the motivation for the work presented in this paper: when gas is injected in a fractured domain and the fractures quickly fill with gas while the matrix blocks are still in single-phase oil, one cannot rigorously define compositional gradients between the fracture and the matrix. As a result, the diffusive cross-flow between fracture and matrix is severely underestimated by simulators that compute the diffusive flux from compositional gradients. This was investigated in detail using the *Eclipse* simulator,[10] where agreement between the experimental data and *Eclipse* simulations could only be achieved by introducing an artificial two-phase grid cell between the fracture and the matrix, with an "inert" component to keep this element in two-phase. Alavian and Whitson[26] also attempted to model this experiment with the *Eclipse 300* simulator but chose to increase the surface (separator) temperature from 15 to 30 °C and decrease the fracture permeability to a low 80 md, which increases the simulated oil recovery through viscous forces to compensate for the limitations in the diffusion modeling. Alavian and Whitson[27] also simulated a similar experiment[28] and again found that the results with and without Fickian diffusion are similar using both

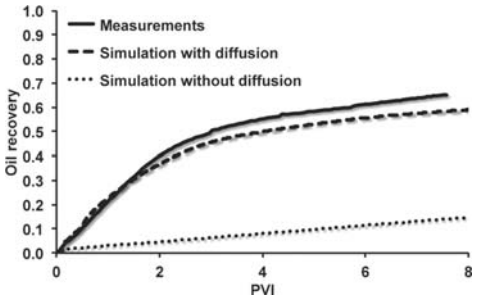

Figure 13. Example 3: Oil recovery.

the *SENSOR* and *Eclipse 300* simulators and that the measured recovery could only be reproduced through viscous forces by lowering the fracture permeability to 26 md. Recent versions of the *Eclipse* simulator do have an option to compute diffusion from chemical potential gradients, but they still suffer from the limitations of the dual-porosity fracture model and the mass balance violations caused by allowing only matrix-diagonal diffusion coefficients, as discussed above.

■ CONCLUSIONS

The main conclusions from this work are as follows:

Fickian diffusion can be important in homogeneous domains as a restoring force for gravitational and viscous flow instabilities. But more importantly, when gas is injected in fractured reservoirs, diffusion can be the main driver of cross-flow between the fractures and the matrix blocks when the fracture intensity is high. Diffusion is often thought to be negligible, because the diffusion coefficients are small and the diffusive fluxes are generally slow compared to the convective flow. However, the main importance of diffusion is to drive species exchange across phase boundaries, that is, over a small length-scale. For example, once CO_2 enters a matrix block, it may reduce the oil viscosity, which increases the *convective* flow of oil in the matrix blocks. At the same time, local dissolution of CO_2 can swell the oil volume, which expels oil from the entire matrix block, that is, beyond the CO_2 invaded region. Through these combined effects, the oil recovery by gas injection with pronounced phase behavior in fractured reservoirs may be considerably higher than what a simulator without a self-consistent model for Fickian diffusion would predict.

The first step in modeling Fickian diffusion rigorously is to take into account the full matrix of composition dependent diffusion coefficients. This is the only approach that does not violate molar balance, and that can describe the nonideality of petroleum fluids in which the diffusive flux of one component is coupled to the flux of all other components.

The main purpose of this work is to resolve a major deficiency of conventional models in which gradients in composition are the driving force for Fickian diffusion. This approach suffers from a numerical issue in multiphase flow when sharp phase boundaries occur at element edges. This often occurs in fractured domains, when the fractures fill with injected gas while the matrix blocks are still in single-phase oil. The compositional gradients are generally computed by differencing the compositions in neighboring grid cells, but this procedure is ill-defined in multiphase flow when a phase is absent in one of the two grid cells. As a result, the effect of diffusion is severely underestimated in simulators relying on this approach. We implement an alternative formulation in which gradients in chemical potentials are the driving force. This formulation is mathematically equivalent to the conventional approach but overcomes this numerical issue, because the chemical potentials are the same in all phases, and gradients in chemical potential can always be defined between two neighboring grid cells.

■ APPENDIX

Discretization of Diffusive Flux Across Grid Edges

To compute the diffusive flux across an edge E between two grid elements K^1 and K^2 (Figure 1), we first discretize the chemical potential gradient in each element as

$$\nabla\mu^1 = \frac{\mu^E - \mu^1}{\Delta x^1/2} \quad \text{and} \quad \nabla\mu^2 = \frac{\mu^2 - \mu^E}{\Delta x^2/2} \tag{25}$$

where μ^1 and μ^2 are the chemical potentials computed from the phases-split computations in elements K^1 and K^2, respectively, and $\Delta x^1/2$ and $\Delta x^2/2$ are the distances from E to the element centers. μ^E is the unknown chemical potential at the edge E. An important advantage of working with chemical potentials rather than compositions is that, because of local thermodynamic equilibrium at the interface (edge) E, $\mu^E = \mu^{1,E} = \mu^{2,E}$, even when K^1 is a gas-filled fracture element and K^2 an undersaturated matrix element. Because of this local thermodynamic equilibrium and the continuity of the diffusive flux, the computation of μ^E can be avoided, as we discuss next.

To simplify the notation, we define the matrices:

$$\tilde{L}_{\alpha,ij} = -\frac{2\phi S_\alpha c_\alpha}{RT\Delta x}\mathcal{B}^{\mathrm{M}}_{\alpha,ij}x_{\alpha,j} \quad \text{and} \quad \tilde{L}_{ij} = \sum_\alpha \tilde{L}_{\alpha,ij} \tag{26}$$

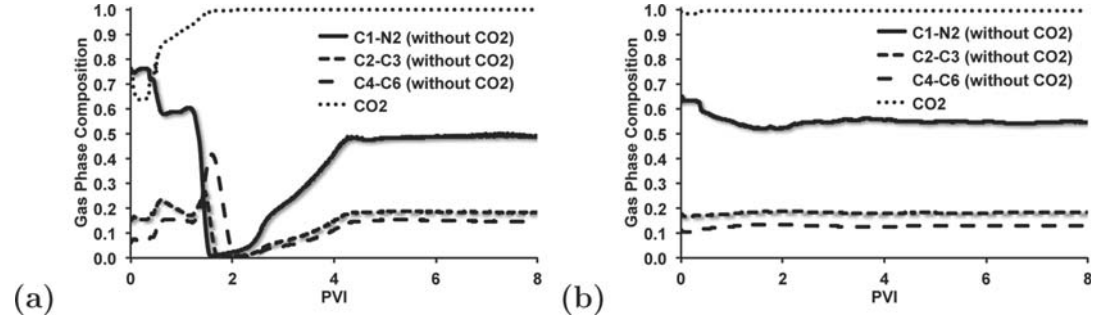

Figure 14. Example 3: Composition (molar fraction) in the produced gas phase at surface conditions for CO_2 and for C_1-N_2, C_2-C_3 and C_4-C_6 after subtracting CO_2. Simulations with diffusion (a) and without Fickian diffusion (b).

dx.doi.org/10.1021/ef401141q | *Energy Fuels* 2013, 27, 5793−5805

Continuity of the total diffusive flux for each component i across the edge E between the two grid elements K^1 and K^2 implies

$$\sum_\alpha J^1_{\alpha,i} = \sum_\alpha J^2_{\alpha,i} \quad \text{or} \tag{27}$$

$$\tilde{\mathrm{L}}^1(\mu^E - \mu^1) = \tilde{\mathrm{L}}^2(\mu^2 - \mu^E) \tag{28}$$

where the superscripts denote the elements K^1 and K^2, and we have used the fact that $\mu_\alpha = \mu$ in the second (matrix) equation. From eq 28 we can ready eliminate μ^E by

$$\mu^E = (\tilde{\mathrm{L}}^1 + \tilde{\mathrm{L}}^2)^{-1}(\tilde{\mathrm{L}}^1\mu^1 + \tilde{\mathrm{L}}^2\mu^2) \tag{29}$$

such that

$$\sum_\alpha \mathbf{J}^1_\alpha = \sum_\alpha \mathbf{J}^2_\alpha = \tilde{\mathrm{L}}^2(\tilde{\mathrm{L}}^2 + \tilde{\mathrm{L}}^1)^{-1}\tilde{\mathrm{L}}^1(\mu^2 - \mu^1) \tag{30}$$

Note that eq 30 is simply the finite difference in chemical potentials between neighboring elements, multiplied by the (matrix) harmonic average of the coefficients. While this is the most self-consistent approach to obtain the coefficients at grid edges, it involves a computationally expensive matrix inversion $(\tilde{\mathrm{L}}^2 + \tilde{\mathrm{L}}^1)^{-1}$. In all applications we have simulated thus far, we find that an arithmetic average $(\tilde{\mathrm{L}}^1 + \tilde{\mathrm{L}}^2)/2$ yields nearly indistinguishable results. We also emphasize that the constraint eq 27 is more general than requiring $j^1_{g,i} = j^2_{g,i}$ and $j^1_{o,i} = j^2_{o,i}$, which is usually done in the conventional approach. If, for example, K^1 is in two-phase and K^2 is single-phase gas, we only assume local thermodynamic equilibrium at E with (unknown) chemical potentials μ^E_i and find $j^1_{g,i} + j^1_{o,i} = j^2_{g,i}$ from eq 30. In the pathological case where K^1 is single-phase gas and K^2 is single-phase oil, we simply have $j^1_{g,i} = j^2_{o,i}$.

What remains is the computation of the difference in chemical potentials $(\mu^2_i - \mu^1_i)$ for each species i. As part of the phase-split computations, we compute the fugacities $f_i(T,p,x_i)$ at constant temperature, pressure, and overall composition. For each element we can write

$$\mu_i^1(T, p^1, x_i^1) = \tilde{\mu}_i^1(T, p^1) + RT \ln f_i^1(T, p^1, x_i^1) - RT \ln \tilde{f}_i^1(T, p^1) \tag{31}$$

and

$$\mu_i^2(T, p^2, x_i^2) = \tilde{\mu}_i^2(T, p^2) + RT \ln f_i^2(T, p^2, x_i^2) - RT \ln \tilde{f}_i^2(T, p^2) \tag{32}$$

The tilde denotes the chemical potential and fugacity of a reference state. If we choose a reference state that is the same in elements K^1 and K^2 (for instance for the pure component i at surface temperature and pressure), these terms drop out when we evaluate the *gradient* in chemical potential between neighboring elements. We therefore implement

$$\begin{aligned}\mu_i^2(T, p^2, x_i^2) - \mu_i^1(T, p^1, x_i^1) &= RT \ln\left(\frac{f_i^2(T, p^2, x_i^2)}{f_i^1(T, p^1, x_i^1)}\right) \\ &= RT \ln\left(\frac{\varphi_i^2 x_i^2}{\varphi_i^1 x_i^1}\right)\end{aligned} \tag{33}$$

where the last expression is in terms of the fugacity coefficients: $\varphi_i = f_i/(x_i p)$. A subtlety here is that Fickian diffusion is driven by variations in compositions at constant temperature and pressure, while variations in temperature and pressure may cause thermal and pressure diffusion, respectively. In numerical implementations, however, the gradients in chemical potentials are computed by differencing chemical potentials in grid cells which may have different pressures. A similar issue occurs in the conventional approach, where the diffusion coefficients (in particular, the non-ideality factor Γ) are computed at different pressures. To reduce this pressure dependence, we have assumed in the last expression in eq 33 that the chemical potential gradient is evaluated at the pressure on edge E, such that the pressures $p^1 = p^2 = p^E$ cancel in the fugacity ratio. The fugacity coefficients φ_i still have some pressure dependence, but this is negligible to the composition dependence over the short distance between two neighboring grid cells.

Just as is customary for the Fickian diffusion coefficients, we project the Onsager coefficients L^1 and L^2, computed from the compositions in the neighboring elements onto their shared edge E, as in eq 30. The phenomenological coefficients are smoother functions of compositions than the Fickian diffusion coefficients (which include the highly nonlinear Γ coefficients), which makes the use of average coefficients at the interface a better approximation. We acknowledge that this is an approximation, and a more rigorous approach would be to simultaneously solve for the fugacities and Fickian diffusive and convective fluxes across a phase boundary.[29] However, the latter formulation involves additional phase-split computations, which is computationally inefficient in the context of large-scale reservoir simulations. Another alternative is to choose the coefficients from the upwind direction with respect to the diffusive flux, as is done in some commercial simulators. However, this is only possible when only the matrix-diagonal self-diffusion coefficients are considered. When the full matrix of diffusion coefficients is used (to avoid mass balance violations), using upwind directions is unfeasible because the diffusive flux of species i depends on the gradients in compositions of *all* components (and all diffusion coefficients). As outline above, the directions of the diffusive fluxes cannot be determined *a priori* from the gradients in chemical potential of each species i alone due to dragging effects.

AUTHOR INFORMATION

Corresponding Author

*E-mail: jmoortgat@rerinst.org; af@rerinst.org.

Notes

The authors declare no competing financial interest.

ACKNOWLEDGMENTS

This work was supported by the member companies of the Reservoir Engineering Research Institute (RERI). Their support is greatly appreciated. We also acknowledge the early contributions to this work by Mohammad Moravvej Farshi at the University of Chicago.

REFERENCES

(1) Hoteit, H.; Firoozabadi, A. *SPE J.* **2009**, *14*, 323−337.
(2) Hoteit, H. *J. Petrol. Sci. Eng.* **2013**, *105*, 1−17.
(3) Leahy-Dios, A.; Firoozabadi, A. *AIChE J.* **2007**, *53*, 2932−2939.
(4) Moortgat, J.; Firoozabadi, A. *Adv. Water Resour.* **2010**, *33*, 951−968.
(5) Duncan, J. B.; Toor, H. L. *AIChE J.* **1962**, *8*, 38−41.

(6) Krishna, R.; Standart, G. *Chem. Eng. Commun.* **1979**, *3*, 201−275.
(7) Ghorayeb, K.; Firoozabadi, A. *SPE J.* **2000**, *5*, 158−171.
(8) Darvish, G.; Lindeberg, E.; Holt, T.; Utne, S. *Laboratory Experiments of Tertiary CO_2 Injection into a Fractured Core*. Presented at the SPE/DOE Symposium on Improved Oil Recovery held in Tulsa, Oklahoma, U.S.A., 22−26 April, 2006.
(9) Darvish, G.; Lindeberg, E.; Holt, T.; Utne, S.; Kleppe, J. *Reservoir-Conditions Laboratory Experiments of CO_2 Injection into Fractured Cores*. Presented at the SPE Europe/EAGE Annual Conference and Exhibition held in Vienna, Austria, 12−15 June, 2006.
(10) Darvish, G. *Physical Effects Controlling Mass Transfer in Matrix Fracture System During CO_2 Injection into Chalk Fractured Reservoirs*. Ph.D. Dissertation 2007:72; Norwegian University of Science and Technology: Trondheim, Norway, 2007.
(11) Peng, D.-Y.; Robinson, D. B. *Ind. Eng. Chem. Fundam.* **1976**, *15*, 59−64.
(12) Moortgat, J.; Firoozabadi, A. *J. Comput. Phys.* **2013**, *250*, 425−445.
(13) Hoteit, H.; Firoozabadi, A. *Adv. Water Resour.* **2008**, *31*, 891−905.
(14) Geiger, S.; Matthäi, S.; Niessner, J.; Helmig, R. *SPE J.* **2009**, *14*, 338−354.
(15) Hoteit, H.; Firoozabadi, A. *SPE J.* **2006**, *11*, 341−352.
(16) Acs, G.; Doleschall, S.; Farkas, E. *SPE J.* **1985**, *25*, 543−553.
(17) Watts, J. W. *SPE Reservoir Eng.* **1986**, *1*, 243−252.
(18) Moortgat, J.; Li, Z.; Firoozabadi, A. *Water Resour. Res.* **2012**, *48*, W12511.
(19) Li, Z.; Firoozabadi, A. *AIChE J.* **2009**, *55*, 1803−1813.
(20) Moortgat, J.; Firoozabadi, A. *SPE J.* **2013**, DOI: 10.2118/159777-PA.
(21) Moortgat, J.; Firoozabadi, A.; Li, Z.; Espósito, R. *SPE J.* **2013**, *18*, 331.
(22) Lohrenz, J.; Bray, B. G.; Clark, C. R. *J. Pet. Technol.* **1964**, *16*, 1171−1176.
(23) Christensen, P.; Pedersen, K. *Phase Behavior of Petroleum Reservoir Fluids*; CRC Press: Boca Raton, FL, 2006.
(24) Dria, D.; Pope, G.; Sepehrnoori, K. *SPE Reservoir Eng.* **1993**, *8*, 143−150.
(25) Firoozabadi, A.; Ishimoto, K. *SPE Adv. Technol. Ser.* **1994**, *2*, 35−44.
(26) Alavian, S.; Whitson, C. *Modeling Miscible CO_2 Injection in a Fractured-Chalk Experiment*. Paper SPE-135339-MS Presented at the SPE Annual Technical Conference and Exhibition, 19−22 September, Florence, Italy, 2010.
(27) Alavian, S.; Whitson, C. *J. Pet. Sci. Eng.* **2011**, *77*, 172−182.
(28) Karimaie, H. *Aspects of Water and Gas Injection in Fractured Reservoir*. Ph.D. Dissertation 2007; Norwegian University of Science and Technology: Trondheim, Norway, 2007.
(29) Rongy, L.; Haugen, K. B.; Firoozabadi, A. *AIChE J.* **2012**, *58*, 1336−1345.